

layer dominated by horizontal flow and emphasize the unique character of the two superplume regions, for which we bring additional evidence of large-scale upwelling. Although measurements of deformation at the pressures and temperatures corresponding to the CMB region are not yet available, our results suggest that similar relationships between anisotropic signature and flow prevail in the uppermost and lowermost mantle.

References and Notes

1. T. Lay, Q. Williams, E. J. Garnero, *Nature* **392**, 461 (1998).
2. S.-I. Karato, *Earth Planets Space* **50**, 1019 (1998).
3. J.-M. Kendall, P. G. Silver, *Nature* **381**, 409 (1996).
4. L. P. Vinnik, V. Farra, B. Romanowicz, *Geophys. Res. Lett.* **16**, 519 (1989).
5. T. Lay, Q. Williams, E. J. Garnero, L. Kellogg, M. Wyssession, in *The Core-Mantle Boundary Region*, M. Gurnis, M. E. Wyssession, E. Knittle, B. A. Buffett, Eds. (American Geophysical Union, Washington, DC, 1998), pp. 219–318.
6. S. A. Russell, T. Lay, E. J. Garnero, *J. Geophys. Res.* **104**, 13183 (1999).
7. C. Thomas, J.-M. Kendall, *Geophys. J. Int.* **151**, 296 (2002).
8. M. S. Fouch, K. M. Fischer, M. E. Wyssession, *Earth Planet. Sci. Lett.* **190**, 167 (2001).
9. X. D. Li, B. Romanowicz, *Geophys. J. Int.* **121**, 695 (1995).
10. C. Mégnin, B. Romanowicz, *Geophys. J. Int.* **143**, 709 (2000).
11. Our data set consists of three-component long-period seismograms (minimum period of 60 s for surface waves and 32 s for body waves) inverted in the time domain in the framework of nonlinear asymptotic coupling theory (9). In this normal-mode perturbation-based approach, we calculate two-dimensional great-circle sensitivity kernels that account for the distribution of sensitivity along and in the vicinity of the ray when using finite-frequency waveform data. Additionally, this approach allows us to use diffracted waves as well as simultaneously arriving phases, which is not possible when using ray theory– and travel time–based approaches (fig. S1 and SOM text).
12. Our model is parameterized in terms of radial anisotropy, which is usually described by density ρ , and five elastic coefficients ($A = \rho V_{P,H}^2$, $C = \rho V_{P,V}^2$, $L = \rho V_{S,H}^2$, $N = \rho V_{S,V}^2$, and F). We chose to describe this equivalently in terms of the isotropic P and S velocities [$V_{P,iso}^2 = 1/5(V_{P,H}^2 + 4V_{P,V}^2)$ and $V_{S,iso}^2 = 1/3(V_{S,H}^2 + 2V_{S,V}^2)$] and three anisotropic parameters [$\xi = N/L$, $\phi = C/A$, and $\eta = F/(A - 2L)$]. The isotropic velocities are derived from the Voigt average isotropic elastic properties (24). These can be expressed as $\rho V_P^2 = (1/15)[3C + (8 + 4\eta)A + 8(1 - \eta)L]$ and $\rho V_S^2 = (1/15)[C + (1 - 2\eta)A + (6 + 4\eta)L + 5N]$. Because in this approach we assume anisotropy to be small, we can simplify the kernel calculation by using $\eta \approx 1$ and $A \approx C$ to reduce the Voigt average expressions to the ones used above. To reduce the number of free parameters in the inversion, we assume the following scaling relationships: $\delta \ln(V_{P,iso}^2) = 0.5 \delta \ln(V_{S,iso}^2)$, $\delta \ln(\eta) = -2.5 \delta \ln(\xi)$, $\delta \ln(\phi) = -1.5 \delta \ln(\xi)$, and $\delta \ln(\rho) = 0.3 \delta \ln(V_{S,iso}^2)$. Scaling relations for the anisotropic parameters have been determined in the laboratory only for conditions down to 500 km (25), so we also performed a lower resolution inversion where ξ , ϕ , and η were allowed to vary independently. The structure in ξ changed very little, and analysis of the resolution matrix indicated that ξ was indeed the best resolved of the three parameters, and tradeoffs were not too strong (fig. S2). The model was parameterized with 16 splines radially, and with spherical harmonics horizontally up to degree 16 for $V_{S,iso}$ and degree 8 for ξ .
13. We performed several tests using the resolution matrix calculated for an inversion up to degree 16 in both V_S and ξ . Tests with a random input model with a white wavelength spectrum indicate that we are capable of correctly resolving the long-wavelength ξ structure with some resolution at

- shorter wavelengths in the upper and lowermost mantle (fig. S3), but not in the bulk of the lower mantle. On this basis, we limited our inversion to degree 8 in ξ . Statistical tests also demonstrate improvement in fit significant at a 95% confidence level for the CMB-sensitive portion of the data set for the model with ξ structure in the lowermost 400 km of the mantle compared to an isotropic model (SOM text).
14. J.-P. Montagner, T. Tanimoto, *J. Geophys. Res.* **96**, 20337 (1991).
15. G. Ekström, A. M. Dziewonski, *Nature* **394**, 168 (1997).
16. Y. Gung, M. Panning, B. Romanowicz, *Nature* **422**, 707 (2003).
17. A. M. Dziewonski, D. L. Anderson, *Phys. Earth Planet. Inter.* **25**, 297 (1981).
18. G. Masters, S. Johnson, G. Laske, B. Bolton, *Philos. Trans. R. Soc. London Ser. A* **354**, 1385 (1996).
19. Y. J. Gu, A. M. Dziewonski, W. Su, G. Ekström, *J. Geophys. Res.* **106**, 11169 (2001).
20. As shown by resolution tests, only the long-wavelength features of our model are well constrained (13). Moreover, we have ignored azimuthal anisotropy, which may influence the details of our model, although radial an-

- isotropy has been shown to adequately describe the data in many of the regional studies (5).
21. A. K. McNamara, P. E. van Keken, S.-I. Karato, *Nature* **416**, 310 (2002).
22. L. Stixrude, in *The Core-Mantle Boundary Region*, M. Gurnis, M. E. Wyssession, E. Knittle, B. A. Buffett, Eds. (American Geophysical Union, Washington, DC, 1998), pp. 83–96.
23. E. Knittle, R. Jeanloz, *Science* **251**, 1438 (1991).
24. V. Babuska, M. Cara, *Seismic Anisotropy in the Earth* (Kluwer Academic, Boston, 1991).
25. J.-P. Montagner, D. L. Anderson, *Phys. Earth Planet. Inter.* **54**, 82 (1989).
26. M. E. Wyssession, K. M. Fischer, G. I. Al-eqabi, P. J. Shore, I. Gurari, *Geophys. Res. Lett.* **28**, 867 (2001).
27. This is contribution 03-10 of the Berkeley Seismological Laboratory. Supported by NSF grant EAR-9902777.

Supporting Online Material
www.sciencemag.org/cgi/content/full/303/5656/351/DC1
 SOM Text
 Figs. S1 to S7

15 September 2003; accepted 3 December 2003

Siberian Peatlands a Net Carbon Sink and Global Methane Source Since the Early Holocene

L. C. Smith,^{1,2*} G. M. MacDonald,^{1,3*} A. A. Velichko,⁴
 D. W. Beilman,¹ O. K. Borisova,⁴ K. E. Frey,¹ K. V. Kremenetski,^{1,4}
 Y. Sheng¹

Interpolar methane gradient (IPG) data from ice cores suggest the “switching on” of a major Northern Hemisphere methane source in the early Holocene. Extensive data from Russia’s West Siberian Lowland show (i) explosive, widespread peatland establishment between 11.5 and 9 thousand years ago, predating comparable development in North America and synchronous with increased atmospheric methane concentrations and IPGs, (ii) larger carbon stocks than previously thought (70.2 Petagrams, up to ~26% of all terrestrial carbon accumulated since the Last Glacial Maximum), and (iii) little evidence for catastrophic oxidation, suggesting the region represents a long-term carbon dioxide sink and global methane source since the early Holocene.

Ice-core records of atmospheric methane concentration show dramatic peaks in the early Holocene, drawing considerable debate as to their source (1). Expansion of tropical wetlands has emerged as a popular hypothesis (2–5), in part because high-latitude peatlands were not well developed in North America by ~11,000 calendar years ago (11 ka), a period of peak methane concentration. However, the timing and volume of peatland growth in Russia, which contains perhaps half of the world’s peat, is virtually unknown. Published esti-

mates of carbon storage in high-latitude peatlands are poorly constrained but large (180 to 455 Pg C) (6), representing up to ~1/3 of the global soil carbon pool (1395 Pg C) (7). Most are known to have formed since the Last Glacial Maximum and thus represent a major terrestrial carbon sink during the Holocene (8). However, the true magnitude and timing of this sink is poorly known because of insufficient data on peatland distribution through time (9), depth, area, age, and carbon content (6, 10). These uncertainties make it difficult to infer the influence of northern peatlands on Holocene greenhouse gas concentrations and to predict the amount of sequestered carbon that could potentially be mobilized under a warmer Arctic climate through water table lowering, peat oxidation, and CO₂ outgassing (6, 11, 12); biosphere uptake (11, 12); or increased dissolved organic carbon efflux to rivers (13).

¹Department of Geography, ²Department of Earth and Space Sciences, ³Department of Organismic Biology, Ecology and Evolution, University of California, Los Angeles, CA 90095–1524, USA. ⁴Russian Academy of Sciences, Moscow 109017, Russia.

*To whom correspondence should be addressed. E-mail: lsmith@geog.ucla.edu (L.C.S.); macdonal@geog.ucla.edu (G.M.M.)

REPORTS

During summer field campaigns in 1999, 2000, and 2001 (14), we collected 87 peat cores from Russia's West Siberian Lowland (WSL), the world's largest peatland complex (6) (Fig. 1). These campaigns were directed at previously unstudied peatlands of the WSL, particularly in permafrost (15). Radiocarbon dating of peat material at the base of each core establishes the age of peatland initiation (table S1). These radiocarbon dates, together with a compilation of 139 additional dates gleaned from a variety of published and unpublished sources (16), provide a comprehensive database of peatland initiation for the entire WSL (Fig. 2). Figures 1 and 2 show that WSL peatlands expanded broadly and rapidly in the early Holocene (11.5 to 9 ka), a period previously thought to be unfavorable for northern peatland development (1, 3, 4, 6, 9, 10, 17, 18). The rapidity of this expansion directly contradicts a "steady-state" peatland growth model previously theorized for the region (18), and the timing of maximum expansion is coincident with peak values of atmospheric methane concentration as recorded in Greenland Ice Sheet Project 2 (GISP2) and Taylor Dome ice cores (Fig. 2).

There are several reasons to believe that Siberian peatlands were a contributing source to the high atmospheric methane concentrations of the early Holocene. First, field experiments confirm that the WSL is a global source of methane today (19, 20). Second, box-model studies of the inter-polar methane gradient (an indicator of the latitudinal distribution of methane sources, computed from the difference between Greenland and Antarctic ice core methane concentrations) strongly suggest existence of a Northern Hemisphere methane source (17, 21, 22). Figure 2 shows a sharp increase (88 to 164%, or 30 to 41 Tg year⁻¹) in Northern Hemisphere emissions during the early Holocene Preboreal period (9.5 to 11.5 ka) as compared with the Last Glacial Maximum (17, 21) (tropical sources also rose by 79 to 89%, or 53 to 58 Tg year⁻¹). This new Northern Hemisphere methane source was not present during either the Younger Dryas (11.5 to 12.5 ka) or Bølling-Allerød (13.5 to 14.8 ka) periods. Third, plausible area-based calculations for possible early Holocene methane fluxes yield large values. Through comprehensive, geographic information system (GIS)-based data inventory (23), we found that WSL peatlands currently occupy ~600,000 km². Inclusion of thin peats (<50 cm) roughly doubles this extent (24). Applying a contemporary flux range (4.2 to 195.3 mg CH₄ m⁻² day⁻¹ for 120 day year⁻¹) (19) to an early Holocene WSL landscape containing just one-half of today's peatlands yields

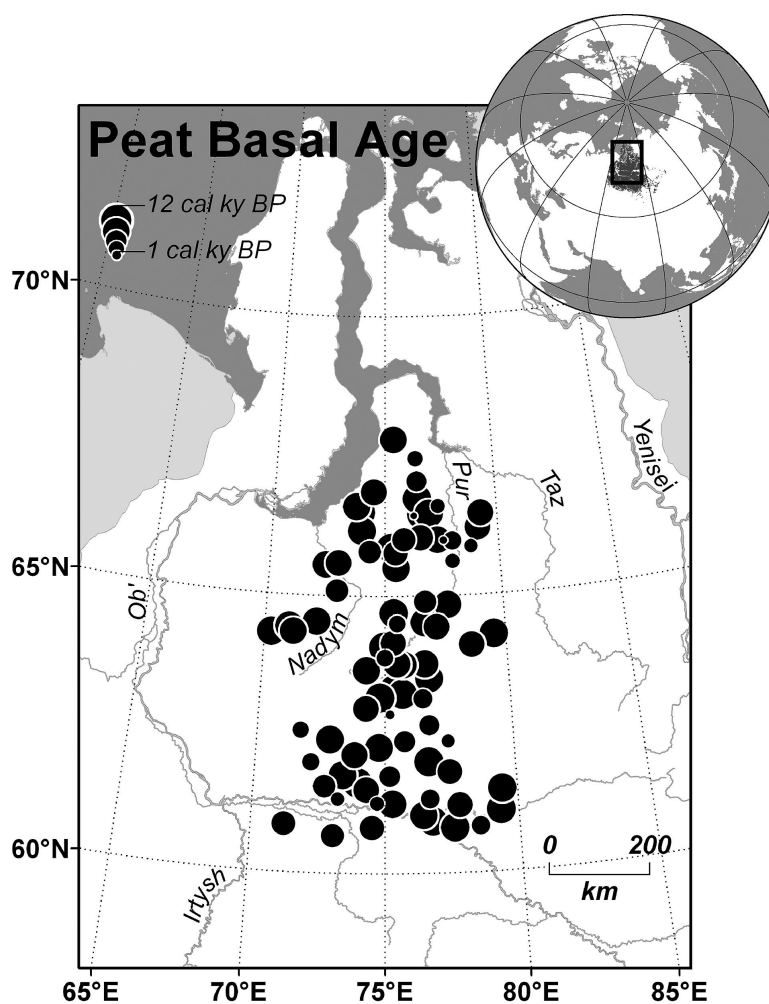


Fig. 1. Location of peat cores drilled in this study. Circle diameters are scaled by basal radiocarbon age. Broad spatial distribution of early Holocene ages [11,500 to 9000 calendar years before present (11.5 to 9 cal ky BP)] confirms that West Siberian peatlands were widely established during this time of high atmospheric methane concentration. Inset shows figure location and geographic extent of our GIS-based peatland inventory.

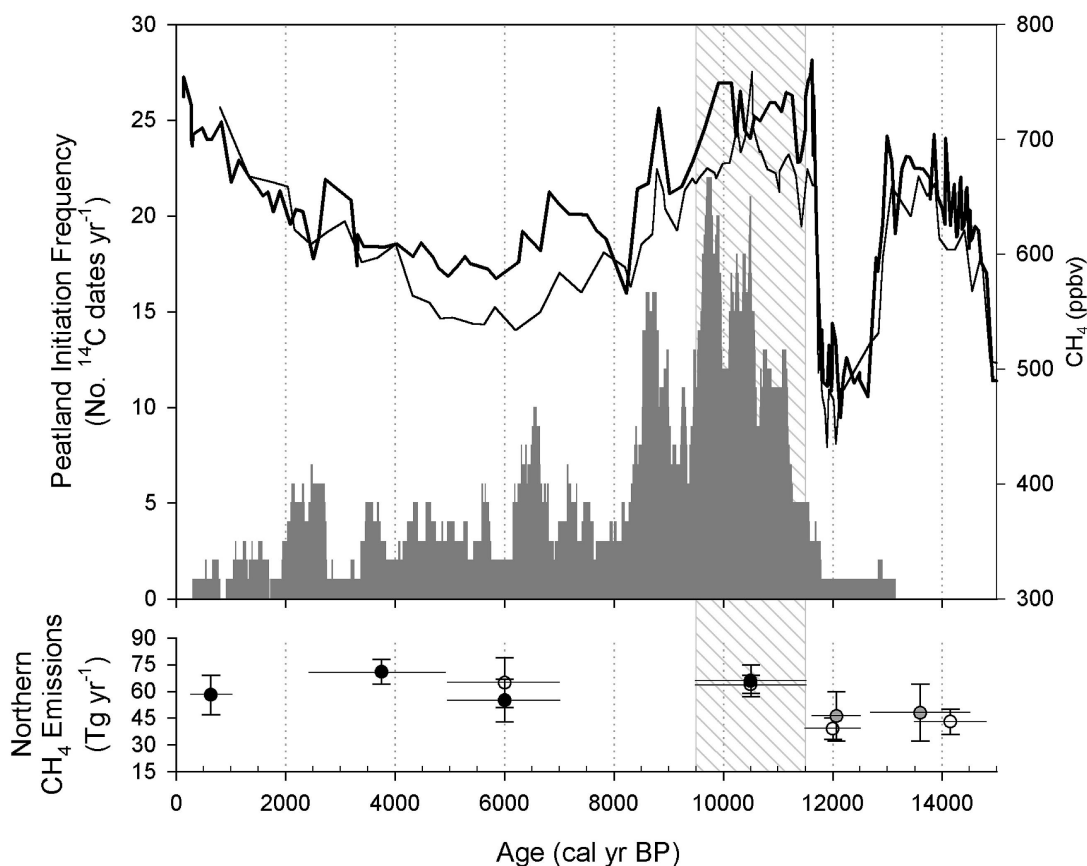
an estimated 0.3 to 14 Tg year⁻¹ CH₄ release from the region. Actual emissions could have been ~six times larger (1.8 to 84 Tg year⁻¹), because, unlike today, macrofossil assemblages in our cores show domination by eutrophic fen species in the early Holocene (25, 26). Furthermore, this calculation ignores completely the possible development of peatlands in central and eastern Siberia, inclusion of which would more than triple the total peatland area to 3.7×10^6 km² today (27).

High-latitude peatlands have been doubted as an early Holocene methane source because of presumed aridity (4), terrestrial glaciation (1–3), and the belief that northern peatlands did not expand substantially until the mid-Holocene (6, 10, 17, 18). These reasons remain largely true for North America. However, it now appears improbable that the WSL was ice-covered during the Last Glacial Maximum (28), and in any event our radiocarbon dates establish

widespread peatland growth there from ~11.5 to 9 ka. Closer inspection of Fig. 2 finds a robust increase in inter-polar methane gradient during the Preboreal period (9.5 to 11.5 ka) as compared with the Younger Dryas (11.5 to 12.5 ka), requiring the "switching on" of ~40 to 65% higher (18 to 25 Tg year⁻¹) Northern Hemisphere methane source in the Preboreal. We believe we have found one such source in Siberia.

Our GIS-based peatland inventory (23) also finds that the WSL peat carbon pool is substantially larger than previously thought, primarily owing to new data from ongoing Russian field survey programs and our extension of coverage beyond that of earlier inventories. Previous estimates range from about 40 to 55 Pg C (27, 24). Our compilation, digitization, and spatial analysis of ~30,000 unpublished Russian measurements of peatland depth, area, bulk density, and ash content, combined with

Fig. 2. Timing of West Siberian peatland establishment and atmospheric methane concentrations (**top**), and northern hemisphere methane emissions derived from the inter-polar methane gradient (IPG) (**bottom**). Occurrence frequency (left vertical axis) of basal peat radiocarbon age ranges (95% confidence level) is plotted with the use of the cumulative probability histogram method (36). Atmospheric methane concentrations (right vertical axis) are from the GISP2 (dark solid line) and Taylor Dome (light solid line) ice cores (21). Northern Hemisphere contributions to the IPG are from Chappellaz *et al.* (17) (solid symbols), Brook *et al.* (21) (open symbols), and Dallenbach *et al.* (22) (gray symbols). Low Northern Hemisphere methane emissions during the Younger Dryas (11.5 to 12.5 ka) and Bølling-Allerød (13.5 to 14.8 ka) indicate atmospheric methane concentrations were driven by tropical sources. However, during the Preboreal (shaded area, 9.5 to 11.5 ka), increased methane concentration and Northern Hemisphere emissions also coincide with rapid and widespread establishment of Siberian peatlands.



our own core, depth, ground-penetrating radar, and visible/near-infrared satellite imagery data, yields a WSL peat carbon pool estimate of 70.2 Pg C. This value is conservative because, like previous investigators (18, 24), we do not consider thin peats (<50 cm) in our inventory. We also assume only 52% peat organic carbon content (after loss on ignition), a more conservative value than is sometimes used (56 to 57% of total peat mass) (10). With a minimum stock of 70.2 Pg C, the WSL represents a substantial Holocene sink for atmospheric CO₂, averaging at least 6.1 Tg C year⁻¹ for the past ~11.5 ka and storing 7 to 26% of all terrestrial carbon accumulated since the Last Glacial Maximum (270 to 1050 Pg C) (12).

Predicting how northern peat carbon stocks may respond to a warming Arctic climate is a complex problem that remains intractable to date. One scenario is that warming will fuel an appreciable new CO₂ source, should currently frozen or waterlogged peats experience warmer temperatures, permafrost degradation, decreased water table elevation, and enhanced aerobic decomposition (6, 11, 12). Such fluxes are potentially large: Assuming no enhanced carbon uptake by the biosphere or ocean, complete oxidation of WSL peatlands over the next 500 years would release ~140 Tg

C year⁻¹ to the atmosphere, boosting the present-day rate of atmospheric CO₂ increase by 0.07 parts per million by volume year⁻¹ (~4% faster than the current rise). In terms of net greenhouse forcing, the warming effect of such a release would likely be offset by reduced methane emission (29) but, even in the unlikely event of a total shutdown of methane emission, would still attain at least ~80% of its greenhouse warming potential (30). Evidence for a recent slowdown or stoppage in WSL peat accumulation does exist (31, 32), and detailed studies of contemporary peat accumulation rates are needed to confirm or disprove this possibility. In the present study, we measured fine debris fraction (<150 μm) (33) throughout our cores to address past decomposition history. We found spatially and temporally varying debris fractions (~25 to 70%) throughout the region but little evidence for a sustained interval of synchronous oxidation (34). Therefore, we doubt occurrence of a past event of massive, region-wide peat oxidation and CO₂ outgassing. However, our evidence for low to moderate decomposition at all depths and latitudes does suggest that most WSL peats have been subjected to varying decomposition, even in current permafrost regions. We therefore suggest

that West Siberian peatlands have behaved primarily as a long-term sink of atmospheric CO₂ and net source of CH₄ since their rapid development in the early Holocene.

References and Notes

1. J. P. Kennett, K. G. Cannariato, I. L. Hendy, R. J. Behl, *Methane Hydrates in Quaternary Climate Change: The Clathrate Gun Hypothesis* (American Geophysical Union, Washington, DC, 2003).
2. J. Chappellaz, J. M. Barnola, D. Raynaud, Y. S. Korotkevich, C. Lorius, *Nature* **345**, 127 (1990).
3. J. Chappellaz *et al.*, *Nature* **366**, 443 (1993).
4. T. Blunier, J. Chappellaz, J. Schwander, B. Stauffer, D. Raynaud, *Nature* **374**, 46 (1995).
5. J. P. Severinghaus, E. J. Brook, *Science* **286**, 930 (1999).
6. E. Gorham, *Ecol. Appl.* **1**, 182 (1991).
7. W. M. Post, W. R. Emanuel, P. J. Zinke, A. G. Stangenberger, *Nature* **298**, 156 (1982).
8. J. W. Harden, E. T. Sundquist, R. F. Stallard, R. K. Mark, *Science* **258**, 1921 (1992).
9. K. Gajewski, A. Viau, M. Sawada, D. Atkinson, S. Wilson, *Global Biogeochem. Cycles* **15**, 297 (2001).
10. M. S. Botch, K. I. Kobak, T. S. Vinson, T. P. Kolchugina, *Global Biogeochem. Cycles* **9**, 37 (1995).
11. W. C. Oechel, G. L. Vourlitis, *Trends Ecol. Evol.* **9**, 324 (1994).
12. G. M. Woodwell *et al.*, *Clim. Change* **40**, 494 (1998).
13. C. Freeman, C. D. Evans, D. T. Monteith, B. Reynolds, N. Fenner, *Nature* **412**, 785 (2001).
14. L. C. Smith *et al.*, *Eos* **497**, 497 (2000).
15. A total of 58 cores were drilled from frozen peat with the use of a gasoline-powered CRREL (Cold Regions Research and Engineering Laboratory) permafrost corer. A total of 29 cores from thawed terrain were taken with a rotating-sleeve Russian peat corer. Basal ages were determined by accelerator mass spectro-

metry and conventional radiocarbon dating of bulk peat samples from the lowest visually apparent peat horizon in each core. Substantially older radiocarbon ages from organic-rich gyttja (mineral substrate) were excluded from new data presented in this paper. Samples were processed by Beta Analytic, Incorporated (Miami, FL) and calibrated with the use of CALIB 4.3 (35) and the Intcal98 data set.

16. X. Kremenetski *et al.*, *Quat. Sci. Rev.* **22**, 703 (2003).
 17. J. Chappellaz *et al.*, *J. Geophys. Res.* **102**, 15987 (1997).
 18. M. I. Neustadt, *Seria Geogr.* **1**, 21 (1971).
 19. J. Heyer, U. Berger, I. L. Kuzin, *Tellus* **54B**, 231 (2002).
 20. E. A. Oberlander *et al.*, *J. Geophys. Res.* **107** (D14), article no. 4206 (2002).
 21. E. J. Brook, S. Harder, J. Severinghaus, E. J. Steig, C. M. Sucher, *Global Biogeochem. Cycles* **14**, 559 (2000).
 22. A. Dallenbach *et al.*, *Geophys. Res. Lett.* **27**, 1005 (2000).
 23. Our estimates of WSL peatland extent (592,440 km²) and total carbon pool (70.2 Pg C) have their basis in a comprehensive GIS-based inventory of all peatlands throughout the region. Data sources assimilated are (i) an archive of printed data reports based on ~40 years of field surveys by Geolortfrazvedka, Moscow, beginning in the 1950s, with updates by the Russian Ministry of Natural Resources in the 1990s. These reports contain detailed maps with associated field and laboratory measurements of peatland depth, area, bulk density, and ash content for 9691 peatlands throughout the WSL, for a total of 29,350 measurements digitized. (ii) Our own field data collected from 1999, 2000, and 2001, including peat physical properties from 87 cores, 78 additional measurements of peatland depth, and 16 ground-penetrating radar transects. (iii) A Russian typological wetland map extending coverage beyond that of the Geolortfrazvedka reports. (iv) Visible/near-infrared MSU-SK satellite images from the Russian RESURS-01 satellite. (v) 62 additional depth measurements gleaned from the published literature. Because of the flat terrain, WSL peatlands are broadly expansive with little depth variation. Ordinary kriging of all available depth data therefore allowed reasonable interpolation of missing values for 3904 of 9691 peatlands inventoried. All data were digitized and incorporated into a ARC 8.2 GIS database and together cover the entire WSL. Total carbon pool (CP) was computed as

$$CP = \left(\sum_{i=1}^n A_i \cdot D_i \cdot r_i \cdot [(100-a_i)/100] \cdot c \right)$$

where n is the number of digitized peat polygons (9691) and A_i , D_i , r_i , a_i , and c represent peatland area, mean depth, depth-averaged bulk density, depth-averaged ash content, and organic carbon fraction (52%), respectively.

24. S. P. Yefremov, T. T. Yefremova, in *West Siberian Peatlands and Carbon Cycle: Past and Present*, S. V. Vasiliev, A. A. Titlyanova, A. A. Velichko, eds. (Agenstvo Sibprint, Novosibirsk, Russia, 2001), pp. 148–151.
 25. The lower (oldest) sections of our cores are dominated by fen species *Scorpidium* sp., *Calliergon* sp., and *Drepanocladus* sp., with later succession to bog species *Sphagnum fuscum* and *S. angustifolium* that dominate the WSL ecology today. Modern transfer function-derived methane fluxes for these fen species average about six times higher than for these bog species (26), suggesting substantially higher WSL methane emission in the early Holocene.
 26. J. L. Bubier, T. R. Moore, S. Juggins, *Ecology* **76**, 677 (1995).
 27. S. E. Vompersky *et al.*, *Pochvovedenie* **12**, 7 (1994).
 28. S. L. Forman, O. Ingolfsson, V. Gataullin, W. F. Manley, H. Lokrantz, *Geology* **27**, 807 (1999).
 29. G. J. Whiting, J. P. Chanton, *Tellus* **53B**, 521 (2001).
 30. Desiccation of WSL peat carbon stocks would elevate atmospheric CO₂ concentrations through peat oxidation but reduce CH₄ emissions through associated drying. Because of high temporal and spatial variability in contemporary rates of CH₄ emission, it is difficult to estimate the potential net radiative balance of these opposing effects. However, even in an

extreme (and unlikely) scenario, assuming (i) complete oxidation of all WSL peat carbon stocks in the next 500 years, (ii) a complete shutdown of all WSL methane emission during the same 500 years, (iii) a 2.5-fold greater infrared absorptivity of CH₄ relative to CO₂ [because of the shorter lifetime of CH₄ in the atmosphere, the greenhouse radiative forcing of CH₄ is only ~2.5 times that of CO₂ when integrated over a 500-year time scale (29)], and (iv) high WSL methane flux at present (~14 Tg CH₄ year⁻¹, calculated as 600,000 km² × 120 day year⁻¹ × 195.3 mg CH₄ m⁻² day⁻¹), the resulting release of ~11.7 × 10¹² mol CO₂ year⁻¹ (from oxidation) would be effectively reduced by 2.2 × 10¹² mol CO₂ year⁻¹ (the radiative equivalent of the loss of 8.7 × 10¹¹ mol CH₄ year⁻¹ emission), or only ~18.8%.

31. D. Peteet, A. Andreev, W. Bardeen, F. Mistretta, *Boreas* **27**, 115 (1998).
 32. J. Turunen, T. Tahvanainen, K. Tolonen, A. Pitkanen, *Global Biogeochem. Cycles* **15**, 285 (2001).
 33. T. J. Malterer, E. S. Verry, J. Erjavac, *Soil Sci. Soc. Am. J.* **56**, 1200 (1992).
 34. Fine debris fraction (percentage of peat fragments ≤150 μm) was measured with the use of the following variation of the ASTM (American Society for Testing Materials) Fiber Weight Method (33). Two-mL peat subsamples were taken every 10 cm throughout all cores, soaked for 12 hours in a dispersing agent (5% sodium hexametaphosphate) and washed through a 150-μm sieve. Coarse debris content (f_{150}) was computed as the ratio of oven-dried mass (100°C) of this fraction relative to that of a complete sample. Percent fine fraction was computed as $(1 - f_{150})$. To identify the possible influence of

species assemblage on f_{150} , we visually assessed macrofossil taxonomies (as percentage of total) with the use of light microscopy. Regression of $(1 - f_{150})$ with core depth and macrofossil abundances within five functional or taxonomic groups (*Sphagnum*, brown moss, sedge, herbaceous, and woody plants) shows that less than 12% of the linear variance in $(1 - f_{150})$ is associated with these factors ($r^2 = 0.114$; $P < 0.0001$), allowing the assumption of external influence (i.e., changing acrotelm temperatures and water table position) on f_{150} .

35. M. Stuiver *et al.*, *Radiocarbon* **40**, 1041 (1998); available at <http://radiocarbon.pa.qub.ac.uk/calib>.
 36. I. D. Campbell, C. Campbell, Z. Yu, D. H. Vitt, M. J. Apps, *Quat. Res.* **54**, 155 (2001).
 37. We thank F. S. Chapin III (University of Alaska, Fairbanks), S. E. Trumbore (University of California, Irvine), and two anonymous readers for constructive reviews. Research funding was provided by NSF through the Russian-American Initiative on Shelf-Land Environments of the Arctic (RAISE) of the Arctic System Science Program (ARCSS). The research presented here was developed jointly by L.C.S. and G.M.M. Numerous Russian scientists, graduate students, and government officials are thanked for their invaluable logistical and scientific support during the Siberian field campaigns.

Supporting Online Material
www.sciencemag.org/cgi/content/full/303/5656/353/DC1
 Table S1

18 August 2003; accepted 1 December 2003

Community Assembly Through Adaptive Radiation in Hawaiian Spiders

Rosemary Gillespie

Communities arising through adaptive radiation are generally regarded as unique, with speciation and adaptation being quite different from immigration and ecological assortment. Here, I use the chronological arrangement of the Hawaiian Islands to visualize snapshots of evolutionary history and stages of community assembly. Analysis of an adaptive radiation of habitat-associated, polychromatic spiders shows that (i) species assembly is not random; (ii) within any community, similar sets of ecomorphs arise through both dispersal and evolution; and (iii) species assembly is dynamic with maximum species numbers in communities of intermediate age. The similar patterns of species accumulation through evolutionary and ecological processes suggest universal principles underlie community assembly.

Community assembly has intrigued biologists for decades (1), leading to a sophisticated understanding of the ecological parameters that dictate community membership (2). The role of evolution in shaping communities is also well appreciated (3, 4), although the steps through which communities are assembled as a result of evolutionary processes have been enigmatic. Adaptive radiations on remote islands provide opportunities to study multiple communities, each

comprising closely related organisms—a feature that has produced insights into evolutionary patterns of species composition and number (5). In particular, two patterns have emerged: (i) A predictable number of species can exist for a given area on remote islands, apparently driven by higher rates of speciation on larger islands (6); and (ii) the end-product of adaptive radiation is often a nonrandom set of species, with lineages diversified in such a way that the same set of ecomorph types occur on each island (7, 8). These findings suggest that evolution on more remote islands can act in a manner analogous to immigration on less remote islands, giving rise to similar spe-

Division of Insect Biology, University of California, 201 Wellman Hall, Berkeley, CA 94720–3112, USA.

*To whom correspondence should be addressed. E-mail: gillespi@nature.berkeley.edu